

Novel numerical method for calculating initial flux of colloid particle adsorption through an energy barrier

Paweł Weroński^{a,b,*}, Menachem Elimelech^c

^a *Theoretical Division and Center for Nonlinear Studies, Los Alamos National Laboratory, MS B284, Los Alamos, NM 87545, USA*

^b *Institute of Catalysis and Surface Chemistry, Polish Academy of Sciences, ul. Niezapominajek 8, 30-239 Kraków, Poland*

^c *Department of Chemical Engineering, Yale University, P.O. Box 208286, New Haven, CT 06520-8286, USA*

Received 11 September 2007; accepted 25 October 2007

Available online 21 December 2007

Abstract

Using variable substitution, we present a general method for the numerical solution of stiff, ordinary, linear, homogeneous differential equations characteristic of colloid particle adsorption/deposition over an energy barrier. For the example of the radial impinging jet system, we demonstrate the application of this method of calculating the colloid concentration profile and initial particle flux in the presence of repulsive electrostatic interactions between the particle and adsorption surface. We show that our method works well in systems with energy barriers up to the order of hundreds of kT , at which point the adsorption flux vanishes. The numerical results obtained with our method are in good agreement with the known limiting analytical approximations for the particle flux through an energy barrier and for a low Péclet number. The developed numerical code is very stable over a wide range of physical parameters, and its accuracy for the most challenging parameter sets is on the order of 10^{-4} . To achieve this stability, we have derived and employed a single formula for the van der Waals dispersion interaction, working at both a small and a large separation distance. We show that this formula converges to the known available analytical expressions for dispersion forces in the limit of small and large separation distance. We also demonstrate that the maximum deviations between our formula and the other equations appear in the intermediate range of the separation distance and do not exceed 10%.

© 2007 Elsevier Inc. All rights reserved.

Keywords: Colloid particle transport; Colloid particle deposition; Convection–diffusion equation; Van der Waals interaction; Modified empirical formula; DLVO theory; Radial stagnation point flow system

1. Introduction

Interactions between colloidal particles in electrolyte solutions and at boundary surfaces, often called collectors, determine the rates of important dynamic phenomena occurring in disperse systems, such as adsorption, deposition (irreversible adsorption), and adhesion [1,2]. A quantitative description of these phenomena has important implications for polymer and colloid science, nanotechnology, biophysics, medicine, and soil chemistry, as well as for many modern technologies involving various separation procedures, such as water and wastewater filtration, membrane filtration, flotation, protein and cell separation, and immobilization of enzymes [3,4].

Because of the great significance of the particle–interface interactions, numerous attempts have been undertaken to quantify these interactions, including the pioneering work of Derjaguin and Landau [5] and Verwey and Overbeek [6], known as the DLVO theory. The foundation of this theory was the postulate of additivity of the dispersion and electrostatic double-layer interactions. The latter were calculated as pair interactions in an infinite electrolyte reservoir using the Poisson equation, with the ion density distribution characterized in terms of the Boltzmann statistics. In this respect, the DLVO theory can be seen as one of many applications of the Gouy–Chapman–Stern [7–9] electric double-layer model. In spite of its simplicity, this model and the DLVO theory have been generally accepted in the scientific community as a reasonable approximation of real experimental systems at low electrolyte and colloid concentrations.

* Corresponding author.
E-mail address: pawel@lanl.gov (P. Weroński).

Once the particle–interface energy profile is known, particle transport can be calculated if the hydrodynamics of the system is not very complicated. Specifically, the colloid concentration and the initial adsorption flux can be found by numerical integration of the continuity equation, also known as the convection–diffusion equation. For a simple geometry of the collector and barrierless adsorption, this equation can be solved using standard numerical techniques [1,10–14]. Under certain simplifying assumptions, approximate analytical solutions are also possible [1,2,15].

This is not the case, however, if the energy profile has an energy barrier and a secondary minimum (SM). Because of the extremely rapidly changing surface forces in the thin boundary layer of the electrolyte, as well as because of the coupling of the particle transport through this thin electrolyte layer with the transport from the bulk, a numerical solution of the convection–diffusion equation becomes a difficult task, which requires the use of sophisticated numerical techniques. Only limited results have been reported so far in the literature for systems with an energy barrier and a secondary minimum [16–19].

Therefore, the goal of this article is to develop a general method for the numerical solution of the convection–diffusion equation in the presence of a very high energy barrier. We will limit our considerations to the radial impinging jet (RIJ) system, also known as the radial stagnation point flow (RSPF) system. The numerical method, however, can in principle be applied to other collector systems involving colloid adsorption/deposition over energy barriers.

2. Theory

2.1. Convection–diffusion equation

Let us consider a dilute suspension of spherical colloid particles in the vicinity of a solid/liquid interface. The particle transport in this system is governed by the continuity equation [1]

$$\frac{\partial n}{\partial t} + \nabla \cdot \mathbf{j} = Q_b, \quad (1)$$

where n is the particle concentration, t is the time, Q_b is the source term describing, e.g., particle aggregation, and \mathbf{j} is the particle flux vector equal to

$$\mathbf{j} = -\mathbf{D} \cdot \nabla n + \mathbf{U}n. \quad (2)$$

The variables \mathbf{D} and \mathbf{U} , appearing in Eq. (2), represent the particle diffusion tensor and the velocity vector, respectively. The latter can be expressed as

$$\mathbf{U} = \mathbf{U}_h + \mathbf{M} \cdot \mathbf{F} + \mathbf{M}_r \cdot \mathbf{T}, \quad (3)$$

where \mathbf{U}_h is the particle velocity due to the hydrodynamic forces alone, \mathbf{M} and \mathbf{M}_r are the translational and rotational mobility matrices, respectively, and \mathbf{F} and \mathbf{T} are the direct force and torque acting on the particle (external and specific). The set of Eqs. (1)–(3) constitutes the so-called convection–diffusion equation, which can be used for modeling colloid particle adsorption at the interface.

Equation (1) needs to be completed by boundary conditions. Far from the interface, the particle concentration n reaches its bulk value n_b . At the interface surface, on the other hand, two different boundary conditions have been applied: (i) the perfect sink (PS) boundary condition, which assumes an infinitely deep primary minimum (PM) of the particle–interface interaction energy at the collector surface, and (ii) the nonpenetration boundary condition, where a finite depth primary energy minimum is assumed. The PS boundary condition, which can be expressed in the form of the equation $n = 0$ at the PM, proved to be a reasonable approximation for calculating the initial adsorption flux in systems with strong particle–collector attraction forces [18], where adsorption can be considered irreversible. If the forces are not strong enough, however, or if one is interested in the kinetics of particle accumulation at the PM, then the second, more general boundary condition has to be applied. This boundary condition can be expressed in the form of the equation $j_n = 0$ at the PM, where j_n is the normal component of the particle flux vector. In this paper we will consider irreversible adsorption and the PS boundary condition only.

If no bulk reaction takes place in the system, the source term Q_b vanishes, and after a very short transition period [18,20], the initial adsorption flux can be calculated from the steady-state convection–diffusion equation,

$$\nabla \cdot [\mathbf{D} \cdot \nabla n - (\mathbf{U}_h + \mathbf{M} \cdot \mathbf{F})n] = 0, \quad (4)$$

where the rotational motion of the particles was neglected.

For a simple geometry of the collector and barrierless adsorption, Eq. (4) can be solved numerically using standard numerical techniques. Under certain simplifying assumptions, analytical solutions are also possible. A detailed discussion of approximate analytical solutions for the convection–diffusion equation can be found in Refs. [1,2,15]. In the case of the RIJ system, close to the stagnation point, where the interface is uniformly accessible to particle adsorption and the particle transfer to the interface does not depend on the radial coordinate, Eq. (4) becomes a one-dimensional ordinary differential equation

$$\frac{d\bar{j}_n}{dH} + 2\text{Pe}F_3(H)(H+1)c(H) = 0, \quad (5)$$

where the normal component of the dimensionless particle flux equals

$$\bar{j}_n(H) = \frac{j_n(H)a}{D_\infty n_b} = -F_1(H) \left\{ \frac{dc}{dH} + [\text{Pe}F_2(H)(H+1)^2 - (F_s(H) + F_e)]c(H) \right\}. \quad (6)$$

Here $c = n/n_b$ is the dimensionless particle concentration; $H = h/a$ is the dimensionless particle–interface gap width or separation distance scaled with the particle radius a , where h is the separation distance; $D_\infty = kT/6\pi\eta a$ is the particle diffusion coefficient, where η is the dynamic fluid viscosity; and F_s is the total force acting between the particle and adsorption surface, expressed in kT/a units and calculated from the DLVO theory as the sum

$$F_s = F_{\text{edl}} + F_{\text{vdW}}, \quad (7)$$

where F_{edl} and F_{vdw} are the electric double layer and dispersion force contributions. The term F_e in Eq. (6) is the net gravity and buoyancy force given by the expression

$$F_e = \frac{4}{3}\pi a^3(\rho_p - \rho_l)g, \quad (8)$$

where ρ_p and ρ_l are the densities of the particle and solution, respectively, and g is the acceleration due to the gravity.

The terms F_1 , F_2 , and F_3 , appearing in Eqs. (5) and (6), are the hydrodynamic correction functions for the spherical particle mobility next to a flat wall. The latter can be calculated from the approximate formulae given by Warszyński [21]:

$$F_1(H) = \frac{19H^2 + 4H}{19H^2 + 26H + 4}, \quad (9a)$$

$$F_2(H) = 1 + \frac{1.79}{(0.828 + H)^{1.167}}, \quad (9b)$$

$$F_3(H) = \begin{cases} \frac{1}{0.754 - 0.256 \ln(H)}, & H < 0.137, \\ 1 - \frac{0.304}{(1+H)^3}, & H \geq 0.137. \end{cases} \quad (9c)$$

Last, the term Pe in Eq. (6) is the dimensionless Péclet number relating the rates of convection and diffusion,

$$Pe = \alpha_r(\text{Re}, h_c/r_c) \frac{V_m a^3}{D_\infty r_c^2}, \quad (10)$$

where r_c and h_c are the capillary radius and the distance between the capillary outlet and the adsorption surface, respectively, $V_m = Q/\pi r_c^2$ is the mean linear velocity of the fluid, where Q is the volume flow, $\text{Re} = Q\rho_l/\pi r_c \eta$ is the Reynolds number relating the inertial and viscous forces, and α_r is the flow parameter dependent on the flow intensity and cell geometry that can be obtained by the numerical solution of the Navier–Stokes equation [22,23]. This dependence has been reported by Warszyński as a function of the Reynolds number for several values of the ratio h_c/r_c [21]. Based on the data published in Refs. [21,22], the following fitting functions for the flow parameter can be found:

$$\alpha_r(\text{Re}) = \frac{0.0734\text{Re}^2 + 0.8}{0.01735\text{Re}^{1.5} + 1}, \quad h_c/r_c = 2, \quad (11)$$

and

$$\alpha_r(\text{Re}) = \frac{0.0255\text{Re}^2 + 0.28}{0.000572\text{Re}^{2.3} + 1}, \quad h_c/r_c = 3. \quad (12)$$

It should be noted that Eq. (7) holds for the boundary conditions

$$c = 0 \text{ at } H = H_1 \quad \text{and} \quad c = 1 \text{ at } H \rightarrow \infty, \quad (13)$$

representing the PS approximation, where H_1 is the PM separation distance. In this model, we can calculate the value of the dimensionless initial adsorption flux, often referred to as the Sherwood number Sh , using the equation:

$$Sh = -\bar{j}_n(H_1). \quad (14)$$

We can rewrite Eq. (5) as

$$\frac{d^2c}{dH^2} + g_1(H) \frac{dc}{dH} + g_0(H)c(H) = 0, \quad (15)$$

where the functions g_0 and g_1 are given by

$$g_0(H) = Pe(H+1) \left[(H+1) \left(\frac{F_2(H)}{F_1(H)} \frac{dF_1}{dH} + \frac{dF_2}{dH} \right) + 2 \left(F_2(H) - \frac{F_3(H)}{F_1(H)} \right) - \left(\frac{F_s(H) + F_e}{F_1(H)} \frac{dF_1}{dH} + \frac{dF_s}{dH} \right) \right],$$

$$g_1(H) = PeF_2(H)(H+1)^2 + \frac{1}{F_1(H)} \frac{dF_1}{dH} - (F_s(H) + F_e). \quad (16)$$

Technically, Eq. (15) is an ordinary, linear, homogeneous differential equation of the second order that, because of Eqs. (13), represents a boundary value problem that can only be solved numerically. Numerical integration of Eq. (15), however, can be challenging because of the coupling between the bulk transport (macroscale) and the transport through the thin boundary layer (microscale), where the rapidly changing strong surface interactions have to be taken into account. This is especially the case when an energy barrier and SM exist in the system, which can result in the variation of the particle concentration by many orders of magnitude over a dimensionless separation distance on the order of 10^{-2} . Differential equations of this kind, known as stiff differential equations, require a special treatment. In what follows, we present a general method for the solution of stiff, ordinary, linear, homogeneous differential equations based on a variable substitution that allows calculation of the initial adsorption flux for several collector geometries. We will demonstrate the application of this method with the example of the RIJ system.

2.2. Variable substitution

The key observation for the application of the variable substitution method is that both the particle concentration and separation distance are never negative. Therefore, instead of the variables c and H , we can use the variables

$$x_1 = \ln(H - H_1) \quad \text{and} \quad y_1 = \ln(c), \quad (17)$$

respectively. Thus,

$$H = \exp(x_1) + H_1, \quad (18a)$$

$$c = \exp(y_1), \quad \frac{dc}{dH} = \exp(y_1 - x_1) \frac{dy_1}{dx_1}, \quad (18b)$$

and

$$\frac{d^2c}{dH^2} = \exp(y_1 - 2x_1) \left[\frac{d^2y_1}{dx_1^2} + \frac{dy_1}{dx_1} \left(\frac{dy_1}{dx_1} - 1 \right) \right]. \quad (18c)$$

Using Eqs. (18a)–(18c), we can rewrite Eq. (15) as

$$\frac{df_1}{dx_1} + f_1(x_1)(f_1(x_1) + b_1(x_1)) + c_1(x_1) = 0, \quad (19)$$

where the functions f_1 , b_1 , and c_1 are defined by the equations

$$f_1(x_1) = \frac{dy_1}{dx_1} = \frac{d \ln c}{d \ln(H - H_1)}, \quad (20)$$

$$b_1(x_1) = g_1(H(x_1)) \exp(x_1) - 1, \quad (21a)$$

and

$$c_1(x_1) = g_0(H(x_1)) \exp(2x_1). \quad (21b)$$

The boundary conditions for Eq. (19) can be found from the series expansion of the concentration in the limit of $H \rightarrow H_1$:

$$c(H) \approx c(H_1) + \left. \frac{dc}{dH} \right|_{H_1} (H - H_1) = \left. \frac{dc}{dH} \right|_{H_1} (H - H_1). \quad (22)$$

Therefore,

$$\begin{aligned} \lim_{x_1 \rightarrow -\infty} f_1(x_1) &= \lim_{H \rightarrow H_1} \frac{d \ln c}{d \ln(H - H_1)} \\ &= \lim_{H \rightarrow H_1} \frac{H - H_1}{c(H)} \frac{dc}{dH} = 1. \end{aligned} \quad (23)$$

Moreover, we can deduce that

$$\lim_{x_1 \rightarrow -\infty} b_1(x_1) = -1 \quad \text{and} \quad \lim_{x_1 \rightarrow -\infty} c_1(x_1) = 0. \quad (24)$$

Therefore, from Eq. (19), we get

$$\lim_{x_1 \rightarrow -\infty} \frac{df_1}{dx_1} = 0. \quad (25)$$

We can conclude that the logarithmic variable substitution transforms the stiff, linear, and homogeneous Eq. (15) into a nonstiff, nonlinear, Riccati-type Eq. (19) that, because of the boundary conditions (23) and (25), represents a more tractable initial value problem. The numerical integration of Eq. (19) yields the function $f_1(x_1)$, which in turn can be numerically integrated to give the logarithm of the colloid concentration as a function of the logarithm of the separation distance from the PM.

If the height of the energy barrier exceeds $10^2 kT$, the calculated value of the particle flux through the barrier becomes negligibly small and we can assume a priori that the adsorption flux vanishes. One can still be interested, however, in calculating the concentration profile and particle flux for the separation distance $H > H_2$, where H_2 is the gap width corresponding to the maximum of the energy barrier. In this distance range, the concentration deviates relatively little from the equilibrium Boltzmann distribution $c(H) \propto \exp(-E_s(H))$, where $E_s(H) = -\int_{\infty}^H F_s(H') dH'$ is the potential energy of the particle–interface interaction in kT units and H' is a dummy integration variable. Therefore, it is reasonable to use the variable substitution

$$x_2 = \ln(H - H_2) \quad \text{and} \quad y_2 = \ln(c \exp(E_s)). \quad (26)$$

Thus, the following relationships hold:

$$H = \exp(x_2) + H_2, \quad c = \exp(y_2 - E_s(H(x_2))), \quad (27a)$$

$$\begin{aligned} \frac{dc}{dH} &= \exp(y_2 - x_2 - E_s(H(x_2))) \\ &\times \left[\frac{dy_2}{dx_2} + F_s(H(x_2)) \exp(x_2) \right], \end{aligned} \quad (27b)$$

and

$$\frac{d^2c}{dH^2} = \exp(y_2 - 2x_2 - E_s(H(x_2)))$$

$$\begin{aligned} &\times \left[\frac{d^2y_2}{dx_2^2} + \frac{dy_2}{dx_2} \left(\frac{dy_2}{dx_2} - 1 + 2F_s(H(x_2)) \exp(x_2) \right) \right. \\ &\left. + \left(F_s^2(H(x_2)) + \frac{dF_s}{dH} \right) \exp(2x_2) \right]. \end{aligned} \quad (27c)$$

Substituting Eqs. (27a)–(27c) into Eq. (15), we get

$$\frac{df_2}{dx_2} + f_2(x_2)(f_2(x_2) + b_2(x_2)) + c_2(x_2) = 0, \quad (28)$$

where the functions f_2 , b_2 , and c_2 are defined by the equations

$$f_2(x_2) = \frac{dy_2}{dx_2} = \frac{d \ln(c \exp(E_s))}{d \ln(H - H_2)}, \quad (29)$$

$$b_2(x_2) = (g_1(H(x_2)) + 2F_s(H(x_2))) \exp(x_2) - 1, \quad (30a)$$

and

$$\begin{aligned} c_2(x_2) &= \left[g_0(H(x_2)) + (g_1(H(x_2)) \right. \\ &\left. + F_s(H(x_2)))F_s(H(x_2)) + \frac{dF_s}{dH} \right] \exp(2x_2). \end{aligned} \quad (30b)$$

The boundary conditions for Eq. (28) can be deduced from the assumption of vanishing of the particle flux through the energy barrier. Substituting Eqs. (27a)–(27c) into Eq. (6) and equating the latter to zero, we get, after simple rearrangements, that in the vicinity of the barrier maximum

$$f_2(x_2) = [F_e - PeF_2(H(x_2))(\exp(x_2) + H_2 + 1)^2] \exp(x_2). \quad (31)$$

The value of the first derivative can be calculated from Eq. (28).

Equation (28) is also a nonstiff Riccati-type differential equation that represents an initial value problem. Because of the substitution (26), the function $f_2(x_2)$ changes even slower than $f_1(x_1)$; therefore, we can easily integrate this equation to calculate the function $f_2(x_2)$, and then the concentration profile and particle flux.

2.3. Limiting analytical solutions

Several limiting analytical expressions have been derived in the literature for the initial adsorption flux in the case of uniformly accessible surfaces. Prieve and Ruckenstein [24] studied particle transport to a rotating disk and found the limiting expression for the initial flux of barrierless adsorption when the convection could be neglected. Following their analysis, we can derive the adsorption flux for the RIJ system in the limit of $Re \rightarrow 0$ [25],

$$Sh = c(H_{SFBL}) \left[\int_{H_1}^{H_{SFBL}} \frac{\exp(E_s(H))}{F_1(H)} dH \right]^{-1}, \quad (32)$$

where H_{SFBL} is a separation distance corresponding to the edge of the surface force boundary layer, where both fluid convection and surface forces vanish, and where the normal component of the particle flux is constant. In our code we have chosen this

distance in such a way that $E_s(H_{\text{SFBL}}) = -10^{-3}$, which is on the order of the particle size.

In the case of the particle transport through a high energy barrier the initial adsorption flux can be calculated from the expression [26]

$$\text{Sh} = \left(\frac{1}{2\pi} \frac{dF_s}{dH} \Big|_{H=H_2} \right)^{1/2} F_1(H_2) \exp(-E_s(H_2)) c(H_4), \quad (33)$$

where the separation distance H_4 represents the boundary of the secondary well at which the surface potential vanishes. If the SM is shallow, this boundary is rather diffuse and can be a little hard to define unequivocally. In our code, we assumed that H_4 is equal to the separation distance of the concentration minimum, which usually appears at a distance larger than H_3 (see the results presented in the next section). We have used Eqs. (32) and (33) to validate our numerical code.

2.4. Electrostatic interaction

The particle–plate electrostatic interaction can be modeled using different approximations reported in the literature. For a low surface potential and a thin electrical double layer, one can use the limiting form of the Hogg–Healy–Fuerstenau (HHF) formula when one of the particles' radii tends to infinity [27],

$$E_{\text{edl}}(H) = \frac{\varepsilon a}{2k_{\text{el}}kT} \left\{ \psi_p \psi_i \ln \frac{1 + \exp(-\kappa a H)}{1 - \exp(-\kappa a H)} + \frac{1}{2} (\psi_p^2 + \psi_i^2) \ln [1 - \exp(-2\kappa a H)] \right\}, \quad (34)$$

where E_{edl} is the particle–plate electrostatic interaction potential energy in kT units, ε is the dielectric constant of the solution, ψ_p and ψ_i are the constant surface potentials of the particle and adsorption surface, respectively, k_{el} is the electrostatic constant dependent on the unit system, equal to one in the CGS system and to $(4\pi\varepsilon_0)^{-1}$ in the SI system, where ε_0 is the dielectric permittivity of vacuum, $\kappa = \sqrt{8\pi k_{\text{el}} k_{\text{us}} e^2 I N_A / (\varepsilon kT)}$ is the inverse Debye length, where k_{us} is the proportionality constant, equal to 10^{-3} and 10^3 in the CGS and SI systems, respectively, e is the proton charge, I is the electrolyte ionic strength expressed in mol/dm^3 , and N_A is the Avogadro number.

The electrostatic force can be calculated from the formula

$$F_{\text{edl}}(H) = -\frac{dE_{\text{edl}}}{dH} = \frac{\varepsilon \kappa a^2 \psi_p \psi_i - \frac{1}{2} (\psi_p^2 + \psi_i^2) \exp(-\kappa a H)}{k_{\text{el}} kT \exp(\kappa a H) - \exp(-\kappa a H)}, \quad (35)$$

where the force is expressed in kT/a units.

In real experiments, however, surface potentials can easily exceed 50 mV, and the parameter κa , representing the thickness of the electric double layer, can be smaller than 10. Under such conditions, the assumptions of the HHF formula are violated and another approximation should be used. Therefore, as a primary method for modeling the electrostatic interaction in our code, we have exploited the linear superposition approximation (LSA) described in Ref. [28] with the effective surface potentials calculated according to the method reported by Ohshima

et al. [29]. In this approach, the particle–plate electrostatic interaction energy can be calculated with the limiting form of the equation for the particle–particle interaction when one of the particles' radii tends to infinity,

$$E_{\text{edl}}(H) = \varepsilon a \frac{kT}{k_{\text{el}} e^2} Y_p Y_i \exp(-\kappa a H), \quad (36)$$

where Y_p and Y_i are the effective constant surface potentials of the particle and adsorption surface, respectively, given by

$$Y_p = \frac{8 \text{tgh}(\bar{\psi}_p/4)}{1 + \sqrt{1 - \frac{2\kappa a + 1}{(\kappa a + 1)^2} \text{tgh}^2(\bar{\psi}_p/4)}} \quad \text{and} \\ Y_i = 4 \text{tgh}(\bar{\psi}_i/4), \quad (37)$$

where $\bar{\psi}_p = \psi_p e / kT$ and $\bar{\psi}_i = \psi_i e / kT$ are the dimensionless surface potentials. The electrostatic force between the particle and the adsorption surface in the LSA method is calculated from

$$F_{\text{edl}}(H) = -\frac{dE_{\text{edl}}}{dH} = \varepsilon \kappa a^2 \frac{kT}{k_{\text{el}} e^2} Y_p Y_i \exp(-\kappa a H). \quad (38)$$

2.5. Dispersion interaction

A detailed review of the formulae used for calculating van der Waals interaction can be found in Gregory [30]. Because of the retardation effect, no single expression has been reported so far in the literature that would correctly represent the interaction at both short and long separation distances. Schenkel and Kitchener [31] found a simple empirical formula for two identical spheres, valid for a short distance H , by interpolation between the expressions for the retarded and unretarded interactions. A similar formula was quoted by Ho and Higuchi [32] for the case of two unequal spheres. The particle–plate dispersion interaction at a short separation distance H can be expressed by the limiting form of this equation when one of the particles' radii tends to infinity [30],

$$E_{\text{s-vdW}}(H) = -\frac{A}{6H} \left(\frac{\lambda_r}{\lambda_r + a_1 H} \right), \quad (39)$$

where A is the Hamaker constant; $\lambda_r = \lambda/a$ is the characteristic wavelength of the dispersion interaction scaled with the particle radius, where $\lambda = 100$ nm; and a_1 is a fitting parameter equal to 1.77, 11.116, and 14 in the Schenkel–Kitchener, Ho–Higuchi, and Gregory equations, respectively. The dispersion force at a short particle–plate separation distance can be expressed as

$$F_{\text{s-vdW}}(H) = -\frac{dE_{\text{s-vdW}}}{dH} = -\frac{A \lambda_r}{6H^2} \frac{\lambda_r + 2a_1 H}{(\lambda_r + a_1 H)^2}. \quad (40)$$

At a large particle–plate separation distance, the Czarnecki formula [33] offers a very good approximation of the van der Waals interaction energy,

$$E_{\text{l-vdW}}(H) = -\frac{A}{6} \left[\frac{2.45 \lambda_r}{10\pi} p_1(H) - \frac{2.17 \lambda_r^2}{120\pi^2} p_2(H) + \frac{0.59 \lambda_r^3}{840\pi^3} p_3(H) \right], \quad (41)$$

where the functions p_1 , p_2 , and p_3 are given by

$$\begin{aligned}
 p_1(H) &= \frac{1-H}{H^2} + \frac{3+H}{(2+H)^2}, \\
 p_2(H) &= \frac{2-H}{H^3} + \frac{4+H}{(2+H)^3}, \\
 p_3(H) &= \frac{3-H}{H^4} + \frac{5+H}{(2+H)^4}.
 \end{aligned}$$

The dispersion force at a long particle–plate separation distance can be expressed as

$$\begin{aligned}
 F_{1-\text{vdW}}(H) &= -\frac{dE_{1-\text{vdW}}}{dH} = -\frac{A}{30} \left[\frac{2.45\lambda_r}{\pi} q_1(H) \right. \\
 &\quad \left. - \frac{2.17\lambda_r^2}{3\pi^2} q_2(H) + \frac{0.59\lambda_r^3}{7\pi^3} q_3(H) \right], \quad (42)
 \end{aligned}$$

where the functions q_1 , q_2 , and q_3 are equal to

$$\begin{aligned}
 q_1(H) &= 8 \frac{1+H}{H^3(2+H)^3}, & q_2(H) &= 2 \frac{6+10H+5H^2}{H^4(2+H)^4}, \\
 q_3(H) &= 2 \frac{8+18H+15H^2+5H^3}{H^5(2+H)^5}.
 \end{aligned}$$

In principle, one could directly use Eqs. (40) and (42) to calculate the van der Waals force below and above the switching distance $H_s \approx \lambda_r/\pi$, respectively. The discontinuity of the force and/or its derivatives at the point H_s could lead, however, to instability of the numerical code. Therefore, it is better to modify Eq. (40) or (42) in such a way as to be able to get a single formula for the whole range of the separation distance. In what follows, we present such a modification for the empirical Eq. (40).

It is easy to notice that in the limit of a very large separation distance H , the functions $q_1(H) \gg q_2(H) \gg q_3(H)$ and the dispersion force calculated with Eq. (42) is determined by the leading term

$$F_{1-\text{vdW}}^\infty(H) \approx -\frac{4A}{15} \frac{2.45\lambda_r}{\pi H^5} \propto \frac{1}{H^5}. \quad (43)$$

On the other hand, Eq. (40) in this limit is determined by the term

$$F_{s-\text{vdW}}^\infty(H) \approx -\frac{A}{3} \frac{\lambda_r}{a_1 H^3} \propto \frac{1}{H^3}. \quad (44)$$

Equations (43) and (44) suggest that the origin of the inaccuracy of Eq. (40) in the limit of the large separation distance is a missing term on the order of H^{-5} . In order to achieve a proper convergence of the dispersion force with the separation distance in this limit, we can add a quadratic term into the denominator of the empirical Eq. (40),

$$F_{\text{vdW}}(H) = -\frac{A\lambda_r}{6H^2} \frac{\lambda_r + 2a_1H}{(\lambda_r + a_1H + a_2H^2)^2}, \quad (45)$$

where a_2 is a numerical constant. In the limit of $H \rightarrow \infty$ this function converges to

$$F_{\text{vdW}}^\infty(H) = -\frac{A}{3} \frac{\lambda_r c_1}{a_2^2 H^5} \propto \frac{1}{H^5}, \quad (46)$$

while in the limit of short separation distance the additional quadratic term becomes insignificant and Eq. (45) reduces to

Eq. (40). The coefficient a_2 can be calculated from the comparison of Eqs. (43) and (46):

$$a_2 = \sqrt{\frac{\pi a_1}{1.96}}. \quad (47)$$

The particle–plate dispersion energy can be derived from Eq. (45),

$$\begin{aligned}
 E_{\text{vdW}}(H) &= -\int_\infty^H F_{\text{vdW}}(H') dH' = -\frac{A\lambda_r}{6} \left[\frac{1}{HX(H)} \right. \\
 &\quad \left. + \frac{3a_2}{\Delta} \left(\frac{a_1 + 2a_2H}{X(H)} + 2a_2 I_0(H) \right) \right], \quad (48)
 \end{aligned}$$

where $\Delta = 4a_2\lambda_r - a_1^2$, $X(H) = \lambda_r + a_1H + a_2H^2$, and the integral $I_0(H)$ depends on the particle size:

$$\begin{aligned}
 I_0(H) &= \int_\infty^H \frac{dH'}{X(H')} \\
 &= \begin{cases} \frac{2}{\sqrt{\Delta}} \arctan \frac{a_1+2a_2H}{\sqrt{\Delta}} - \frac{\pi}{2}, & \Delta > 0, \\ -\frac{2}{a_1+2a_2H}, & \Delta = 0, \\ -\frac{1}{\sqrt{-\Delta}} \ln \frac{a_1-\sqrt{-\Delta}+2a_2H}{a_1+\sqrt{-\Delta}+2a_2H}, & \Delta < 0. \end{cases} \quad (49)
 \end{aligned}$$

In our code, we calculated van der Waals forces with Eq. (45), where the value of $a_1 = 11.12$. The coefficient a_2 calculated with Eq. (47) was $a_2 \approx 4.22$. A comparison of the dispersion forces calculated with the different formulae is presented in Fig. 1. Note that the results predicted with Eq. (45) are in very good agreement with the Ho–Higuchi equation at a short separation distance, as well as with the Czarnecki equation at a long separation distance.

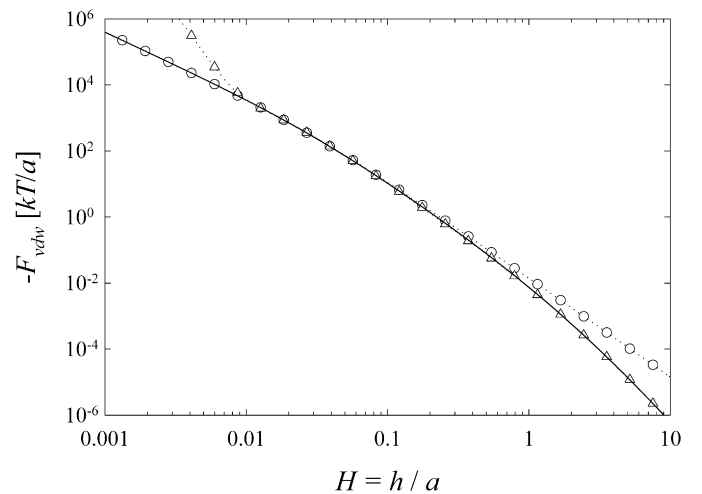


Fig. 1. Comparison of the absolute value of the particle–plate dispersion force calculated with three different formulae: Ho–Higuchi, Eq. (40) with $a_1 = 11.12$ (dotted line with circles); Czarnecki, Eq. (42) (dotted line with triangles); and Eq. (45) (solid line). The interaction force was calculated for a colloid particle size $a = 500$ nm and a flat plate, with a Hamaker constant $A = 2.4$ kT. Note that the results predicted with Eq. (43) are in very good agreement with the Ho–Higuchi equation at short separation distances, as well as with the Czarnecki equation at long separation distances.

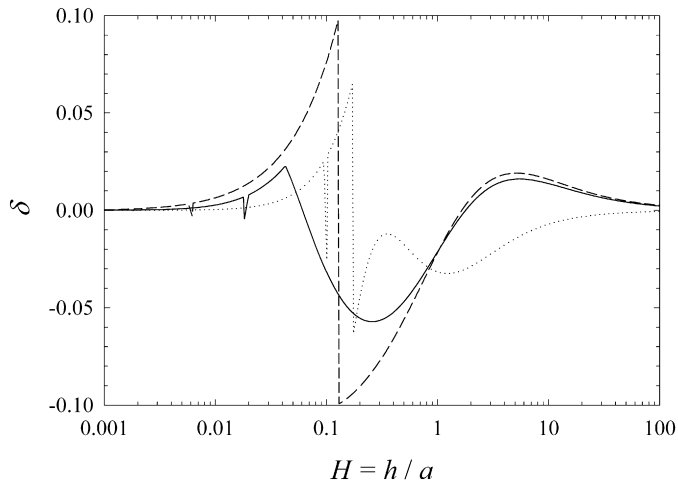


Fig. 2. Relative difference between the dispersion forces calculated with Eqs. (45) and (40) or (42). Dotted, dashed, and solid lines represent results obtained with Eq. (50) for three particle sizes: $a = 50, 500,$ and 5000 nm, respectively. Note the very good agreement in the limits of short and long separation distances. The maximum deviations of the difference δ appear in the range of the intermediate distance H and do not exceed 10%.

The relative difference between the dispersion force calculated with Eqs. (45) and (40) or (42) can be quantitatively evaluated using the function

$$\delta(H) = \begin{cases} \delta_s(H), & |\delta_s(H)| \leq |\delta_l(H)|, \\ \delta_l(H), & |\delta_s(H)| > |\delta_l(H)|, \end{cases} \quad (50)$$

where $\delta_i(H) = F_{i-\text{vdW}}(H)/F_{\text{vdW}}(H) - 1$, $i = s, l$. The numerical results calculated with Eq. (50) for three particle sizes: $a = 50, 500,$ and 5000 nm are presented in Fig. 2. As one can notice, the function $\delta(H)$ converges to zero in the limits of the short and long separation distances. Its maximum deviations appear in the range of the intermediate distance H and do not exceed 10%.

3. Numerical protocols

3.1. Integrating the convection–diffusion equation

Solution of the Riccati equations (19) and (28) is not very demanding; therefore, one can use a variety of standard numerical procedures. In our code, we exploited the subroutine DDASSL [34] by Petzold, which is a part of the open source library SLATEC [35], available on the Internet. This subroutine solves systems of differential algebraic equations using the backward differentiation formula of order 5. The code advances the solution between two subsequent points of the grid, using step sizes that are automatically selected to achieve the desired accuracy. Two of the subroutine's accuracy parameters, a_{tol} and r_{tol} , were set to 10^{-15} and 3×10^{-14} , respectively. All the derivatives appearing in the program were calculated using the analytical formulae derived from the equations in the theoretical part of this paper.

We tested the code on personal computers in a wide range of the physical parameters and found it to be very stable. Numerical parameters, such as the number of grid nodes n_g , as

Table 1
Physicochemical (upper part) and numerical (lower part) parameters used in our simulations

Parameter	Value
Gravitational acceleration, g	9.81 m/s ²
Temperature, T	295 K
Particle radius, a	500 nm
Particle density, ρ_p	1.055 g/cm ³
Particle surface potential, ψ_p	−19.65, 19.65, 28.80 mV
Interface surface potential, ψ_i	20 mV
Primary minimum distance, h_1	0.1 nm
Fluid density, ρ_l	1 g/cm ³
Dynamic fluid viscosity, η	9.35 mP
Solution dielectric constant, ϵ	78.54
Solution ionic strength, I	50 mM
Particle number density, n_b	10 ⁸ /cm ³
Capillary radius, r_c	1 mm
Geometrical factor, h_c/r_c	2
Reynolds number, Re	10 ^{−2}
Flow parameter, α_r	0.8
Péclet number, Pe	2.02 × 10 ^{−6}
Bulk diffusion coefficient, D_∞	4.62 × 10 ^{−9} cm ² /s
Electrostatic screening parameter, κa	370
Hamaker constant, A	10 ^{−20} J
Lower integration limit, h_{min}	(1 + 10 ^{−8}) h_1
Upper integration limit, h_{max}	5 cm
Number of grid nodes, n_g	1000
Absolute error tolerance, a_{tol}	10 ^{−15}
Relative error tolerance, r_{tol}	3 × 10 ^{−14}

well as the lower and upper integration limits, can be a little dependent on the physical parameters of the modeled system and should be chosen empirically to achieve the best accuracy. Generally, however, we found that the optimal value of the lower integration limit was on the order of $x_1^{\text{min}} \approx \ln(H_1) - 16$, which corresponded to the minimum separation distance $H_{\text{min}} \approx (1 + 10^{-8})H_1$. The upper integration limit and the number of the grid nodes depend on the flow intensity. We found that for the Reynolds number $Re \approx 10^{-2}$, the upper integration limit should be on the order of $x_m^{\text{max}} \approx 12$, where $m = 1, 2$, which corresponded to the maximum separation distance $H_{\text{max}} \approx 10^5$. Calculations conducted for this value of the Reynolds number, the parameter $\kappa a = 370$, and the energy difference $E_s(H_2) - E_s(H_3) \approx 36 kT$, where H_3 is the SM distance, suggested that for such integration limits and for $n_g \geq 10^3$, the relative variation of the adsorption flux with the growing number of nodes was in the range of 10^{-4} , which we consider high accuracy. The accuracy increases rapidly with the Reynolds number, the thickness of the electric double layer, and the decrease of the energy barrier.

The physicochemical and numerical parameters used in our simulations are collected in Table 1.

3.2. Calculating the colloid concentration profile and particle flux at the secondary minimum

Once the integrand of Eqs. (19) or (28) had been determined, we calculated the logarithm of the colloid concentration by integration of the interpolating quadratic polynomials that were

obtained for subsequent triplets of the grid nodes. The coefficients of the interpolating polynomials were calculated using the procedure DGEFS [36] by Voorhees, which is available in the library SLATEC [35]. Then the separation distance, the concentration, and its first derivative were calculated at the grid points using Eqs. (18a)–(18c) or (27a)–(27c). Finally, we calculated the normal component of the particle flux with Eq. (6).

The dimensionless surface concentration of the particles trapped in the SM can be calculated by integrating the particle concentration around the SM:

$$\theta = \pi a^3 n_b \int_{H_2}^{H_4} c(H) dH. \quad (51)$$

To calculate the integral appearing in Eq. (51) we used the linear interpolation of the concentration between the grid nodes. For localizing the energy barrier and SM, we used Ridder's method, described in Refs. [37,38].

4. Results and discussion

In this section we present the numerical results obtained for three different systems, without an energy barrier, with a barrier of height $E_s(H_2) = 20 \text{ kT}$, and with an SM of depth $E_s(H_3) \approx -16 \text{ kT}$, as well as for a system with a high energy barrier on the order of $E_s(H_2) = 100 \text{ kT}$. To demonstrate the computational abilities of the code, in all the systems we chose a low Reynolds number, $\text{Re} = 0.01$, and a large parameter $\kappa a \approx 370$. In all of the systems we used the same physicochemical parameters, listed in Table 1, except the particle surface potential, which was equal to $\psi_p = -19.65, 19.65, \text{ and } 28.80 \text{ mV}$, respectively.

Fig. 3 presents the particle–interface interaction energy, colloid concentration, and particle flux as functions of the separation distance, calculated for the system with no energy barrier. The concentration profile decreases monotonically with the separation distance. The linear regime of this profile at the

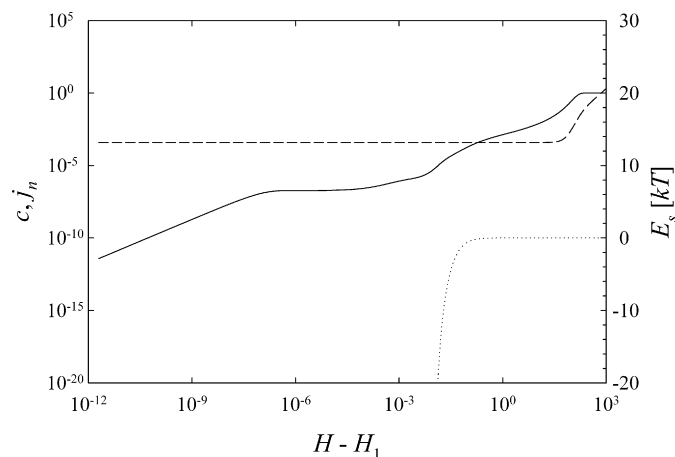


Fig. 3. Particle–interface interaction energy (dotted line), colloid concentration (solid line), and normal component of particle flux (dashed line) as functions of separation distance. At low Reynolds number, the particle flux is constant over a wide range of the separation distance, in agreement with the assumptions made in the derivation of Eq. (32).

lowest distance range corresponds to the linear regime of the integrand $f_1(x_1) \approx 1$, where Eq. (22) holds. Physically, the rectilinear fragment of the concentration profile represents a linear dependence of the concentration on the distance from the primary minimum location. The particle flux is constant for a separation distance $H < 10$, which results from the low flow intensity and confirms the validity of the approximate Eq. (32). Indeed, numerically and analytically calculated values of the adsorption flux, equal respectively to $\text{Sh} = 3.795 \times 10^{-4}$ and 3.919×10^{-4} , differ by just 3%. At a particle–interface separation distance above 10^2 , where the particle–interface interaction vanishes and the concentration achieves its bulk value, we can see that the normal component of the particle flux diminishes with the gap width. This effect is clearly hydrodynamic and results from a nonzero radial component of the particle flux between the capillary outlet and the adsorption surface at the large separation distance. Below the distance 10^2 , the colloid concentration decreases with the separation distance, which suggests that diffusion starts to play a role in this distance range. Indeed, with decreasing particle–wall distance, the convection transport decreases due to the growing hydrodynamic interaction. Overall, however, the normal component of the particle flux stays constant. This means that, at negligible particle–interface interaction, the diffusive particle transport dominates.

Fig. 4 presents more interesting results obtained for the system with the energy barrier of height 20 kT . The particle flux to the PM and SM is constant. The latter is just a result of the negligible convection. The former is a consequence of the very small distance between the energy barrier and the PM, as well as the fact that the barrier is very thin. Therefore, the radial component of the particle flux at the energy barrier is negligibly small, and the normal component of the particle flux through the barrier is constant even for vigorous flows. The numerically calculated adsorption flux is $\text{Sh} = 4.368 \times 10^{-11}$, which is consistent with the approximate analytical result $\text{Sh} = 5.055 \times 10^{-11}$ calculated with Eq. (33). Note that the dimen-

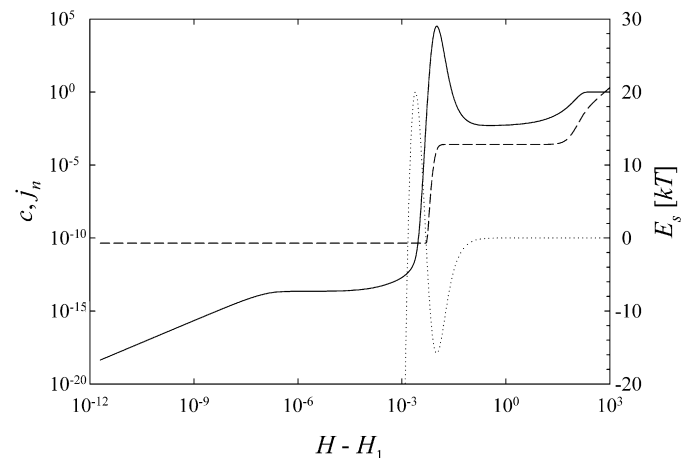


Fig. 4. Particle–interface interaction energy (dotted line), colloid concentration (solid line) and normal component of particle flux (dashed line) as functions of separation distance in the system with an energy barrier of a height of 20 kT . The particle flux to the PM and SM is constant because of the negligible convection and small separation distance between the barrier and the adsorption surface. Note the strong particle accumulation at the SM.

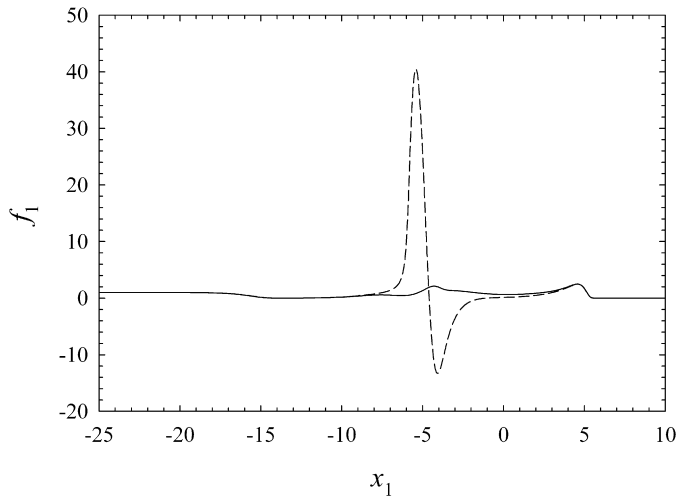


Fig. 5. Comparison of integrand $f_1(x_1)$ calculated for two systems, with and without an energy barrier. The results are depicted by dashed and solid lines, respectively. The function is very smooth in the case of the barrierless deposition and changes more rapidly when the barrier is present. The changes are still relatively slow, and the function can be numerically integrated using the standard techniques.

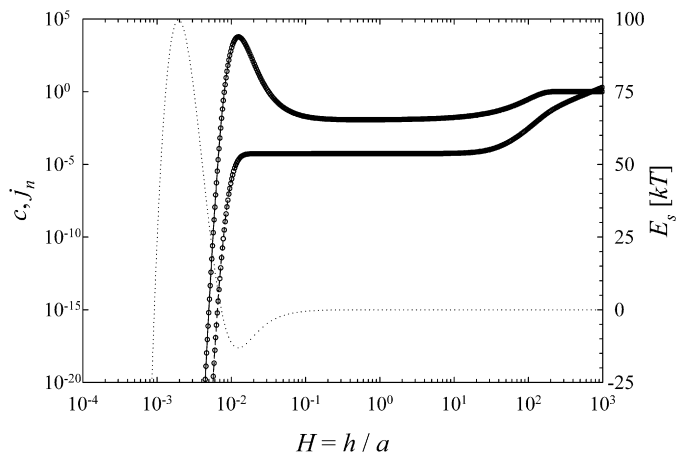


Fig. 6. Comparison of colloid concentration (solid line) and normal component of particle flux (dashed line) calculated with different variable substitutions. Lines and open circles represent the results obtained with Eqs. (17) and (26), respectively. Note that the results are essentially identical. The energy profile for the system with a barrier of a height of 100 kT is depicted by the dotted line.

sionless particle concentration changes rapidly by about 20 orders of magnitude over a dimensionless distance on the order of 10^{-1} , which makes the direct integration of Eq. (15) very hard. The concentration profile has a high maximum corresponding to the energy SM. The particle surface concentration at this minimum, calculated with Eq. (51), is $\theta = 4.64 \times 10^{-2}$. As discussed in the previous paragraph, the linear regime of the concentration profile at the lowest distance range corresponds to the linear regime of the integrand $f_1(x_1) \approx 1$, where Eq. (22) holds. Note that above distances on the order of 10, both the concentration and the normal component of the particle flux are similar to those presented in Fig. 3. This similarity suggests that as long as the secondary minimum is deep enough, the presence of the energy barrier has little effect on the colloid transport far from the interface.

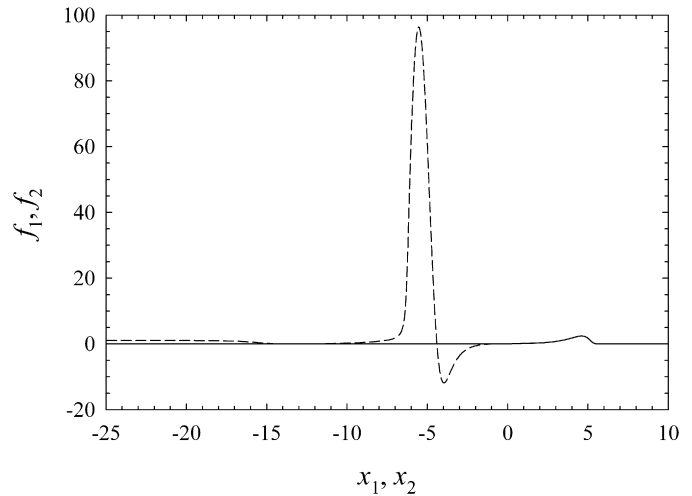


Fig. 7. Comparison of integrands $f_1(x_1)$ (dashed line) and $f_2(x_2)$ (solid line) calculated in a system with a high energy barrier.

A comparison of the integrands $f_1(x_1)$ for the two systems is presented in Fig. 5. The function is very smooth for the system without an energy barrier. The presence of the energy barrier results in more rapid changes of the function at the value of the argument corresponding to the distance of the energy barrier and SM. Even in this system, however, the function changes relatively slowly and can be integrated using the standard numerical techniques.

In Fig. 6 we present the energy profile, colloid concentration, and particle flux calculated for the third system with a very high energy barrier of about 10^2 kT , where the adsorption flux vanishes. The results were obtained using the two different variable substitutions defined by Eqs. (17) and (26). As one can notice, the results are essentially identical. Again, the particle flux to the SM is constant at a distance $H < 10$, and a particle accumulation takes place at the SM. The particle surface concentration at this minimum, calculated with Eq. (51), is $\theta = 9.56 \times 10^{-4}$. This lower value, as compared to the system with the lower energy barrier, results from the shallower SM.

The integrands themselves have been compared in Fig. 7. The function $f_2(x_2)$ varies very little, which confirms the Boltzmann distribution of the colloid concentration at the interface. The variations of the function $f_1(x_1)$ are much larger, but still small enough to allow integration of Eq. (28) with standard numerical techniques.

5. Conclusions

We have developed a general method for numerical solution of stiff ordinary linear homogeneous differential equations, such as those describing colloid particle adsorption over energy barriers, by variable substitution. We have demonstrated the application of this method to calculating the colloid concentration profile and initial particle flux in the RIJ system. We have shown that our method works well in systems with an energy barrier up to the order of hundreds of kT , at which the adsorption flux vanishes. The numerical results obtained with our method are in good agreement with limiting analytical approximations.

The developed numerical code has been very stable over a wide range of physical parameters, and its accuracy at the most challenging parameter sets is of the order of 10^{-4} . To achieve this stability, we have derived and employed a single formula for the dispersion interaction, working in the whole separation distance range $H \in (0; \infty)$. We have shown that this formula converges to the known analytical expressions in the limit of small and large separation distances. We have also demonstrated that the maximum deviations between our formula and the other equations appear in the intermediate range of the separation distance and do not exceed 10%.

Acknowledgments

Funding was provided by the National Science Foundation (BES 0228911). We thank Professor Subir Bhattacharjee for recommending the SLATEC library.

References

- [1] Z. Adamczyk, B. Siwek, M. Zembala, P. Belouschek, *Adv. Colloid Interface Sci.* 48 (1994) 151.
- [2] M. Elimelech, J. Gregory, X. Jia, R. Williams, *Particle Deposition and Aggregation*, Butterworth–Heinemann, Stoneham, MA, 1995.
- [3] S.L. Walker, J.A. Redman, M. Elimelech, *Langmuir* 20 (2004) 7736.
- [4] P. Weroński, J.Y. Walz, M. Elimelech, *J. Colloid Interface Sci.* 262 (2003) 372.
- [5] B.V. Derjaguin, L. Landau, *Acta Phys. Chem.* 14 (1941) 633.
- [6] J.W. Verwey, J.Th.G. Overbeek, *Theory of the Stability of Lyophobic Colloids*, Elsevier, Amsterdam, 1948.
- [7] G. Gouy, *J. Phys.* 9 (1910) 457.
- [8] D.L. Chapman, *Phil. Mag.* 25 (1913) 475.
- [9] O. Stern, *Z. Electrochem.* 30 (1924) 508.
- [10] J.C. Heinrich, P.S. Huyakorn, O.C. Zienkiewicz, A.R. Mitchells, *Int. J. Numer. Methods Eng.* 11 (1977) 131.
- [11] Z. Adamczyk, B. Siwek, M. Zembala, P. Warszyński, *J. Colloid Interface Sci.* 130 (1989) 578.
- [12] Z. Adamczyk, L. Szyk, P. Warszyński, *Colloids Surf. A* 75 (1993) 185.
- [13] M. Elimelech, *J. Colloid Interface Sci.* 164 (1994) 190.
- [14] J. Yang, R. Bos, A. Poortinga, P.J. Wit, G.F. Belder, H.J. Busscher, *Langmuir* 15 (1999) 4671.
- [15] T.G.M. van de Ven, *Colloidal Hydrodynamics*, Academic Press, London, 1989.
- [16] T. Dąbroś, Z. Adamczyk, *Chem. Eng. Sci.* 34 (1979) 1041.
- [17] T. Dąbroś, T.G.M. van de Ven, *Colloid Polym. Sci.* 261 (1983) 694.
- [18] Z. Adamczyk, T. Dąbroś, J. Czarnecki, T.G.M. van de Ven, *J. Colloid Interface Sci.* 97 (1984) 91.
- [19] N. Nazemifard, J.H. Masliyah, S. Bhattacharjee, *Langmuir* 22 (2006) 9879.
- [20] Z. Adamczyk, T.G.M. van de Ven, *J. Colloid Interface Sci.* 97 (1984) 68.
- [21] P. Warszyński, *Adv. Colloid Interface Sci.* 84 (2000) 47.
- [22] Z. Adamczyk, P. Warszyński, L. Szyk-Warszyńska, P. Weroński, *Colloids Surf. A* 165 (1999) 157.
- [23] Z. Adamczyk, L. Szyk, P. Warszyński, *J. Colloid Interface Sci.* 209 (1999) 350.
- [24] D.C. Prieve, E. Ruckenstein, *AIChE J.* 20 (1974) 1178.
- [25] Z. Adamczyk, P. Weroński, *Adv. Colloid Interface Sci.* 83 (1999) 137.
- [26] E. Ruckenstein, D.C. Prieve, *AIChE J.* 22 (1976) 276.
- [27] R. Hogg, T.W. Healy, D.W. Fuerstenau, *Trans. Faraday Soc.* 62 (1966) 1638.
- [28] G.M. Bell, S. Levine, L.N. McCartney, *J. Colloid Interface Sci.* 33 (1970) 335.
- [29] H. Ohshima, T.W. Healy, L.R. White, *J. Colloid Interface Sci.* 90 (1982) 17.
- [30] J. Gregory, *J. Colloid Interface Sci.* 81 (1981) 138.
- [31] J.H. Schenkel, J.A. Kitchener, *Trans. Faraday Soc.* 56 (1960) 161.
- [32] N.F.H. Ho, W.I. Higuchi, *J. Pharm. Sci.* 57 (1968) 436.
- [33] J. Czarnecki, *J. Colloid Interface Sci.* 72 (1979) 361.
- [34] K.E. Brenan, S.L. Campbell, L.R. Petzold, *The Numerical Solution of Initial Value Problems in Differential-Algebraic Equations*, in: *SIAM Classics Series*, SIAM, Philadelphia, 1996.
- [35] Available at: <http://www.netlib.org/slatec/>.
- [36] J.J. Dongarra, J.R. Bunch, C.B. Moler, G.W. Stewart, *LINPACK Users' Guide*, SIAM, Philadelphia, 1979.
- [37] C.J.F. Ridders, *IEEE Trans. Circuits Syst. CAS-27* (1979) 979.
- [38] W.H. Press, S.A. Teukolsky, W.T. Vetterling, B.P. Flannery, *Numerical Recipes in Fortran*, Cambridge Univ. Press, New York, 1992.